ARL-TR-9511 ● AUG 2022

DEVCOM ARMY RESEARCH LABORATORY

Porosity and Void Size Quantification in Carbon Materials with X-ray-Computed Tomography (XCT) and Mercury Infiltration Porosimetry (MIP)

by Jennifer M Sietins, Ngon T Tran, Daniel B Knorr Jr, Jason J Cain, and Keaton W Klaff

NOTICES

Disclaimers

The findings in this report are not to be construed as an official Department of the Army position unless so designated by other authorized documents.

Citation of manufacturer's or trade names does not constitute an official endorsement or approval of the use thereof.

Destroy this report when it is no longer needed. Do not return it to the originator.

ARL-TR-9511 ● AUG 2022

Porosity and Void Size Quantification in Carbon Materials with X-ray-Computed Tomography (XCT) and Mercury Infiltration Porosimetry (MIP)

Jennifer M Sietins, Ngon T Tran, Daniel B Knorr Jr, and Jason J Cain
DEVCOM Army Research Laboratory

Keaton W Klaff
Bennett Aerospace, Inc

REPORT DOCUMENTATION PAGE

Form Approved
OMB No. 0704-0188

1. REPORT DATE *(DD-MM-YYYY)*	2. REPORT TYPE	3. DATES COVERED (From - To)
August 2022	Technical Report	10 October–1 June 2021

4. TITLE AND SUBTITLE
Porosity and Void Size Quantification in Carbon Materials with X-ray-Computed Tomography (XCT) and Mercury Infiltration Porosimetry (MIP)

5a. CONTRACT NUMBER

5b. GRANT NUMBER

5c. PROGRAM ELEMENT NUMBER

6. AUTHOR(S)
Jennifer M Sietins, Ngon T Tran, Daniel B Knorr Jr, Jason J Cain, and Keaton W Klaff

5d. PROJECT NUMBER

5e. TASK NUMBER

5f. WORK UNIT NUMBER

7. PERFORMING ORGANIZATION NAME(S) AND ADDRESS(ES)
DEVCOM Army Research Laboratory
ATTN: FCDD-RLW-MB
Aberdeen Proving Ground, MD 21005

8. PERFORMING ORGANIZATION REPORT NUMBER
ARL-TR-9511

9. SPONSORING/MONITORING AGENCY NAME(S) AND ADDRESS(ES)

10. SPONSOR/MONITOR'S ACRONYM(S)

11. SPONSOR/MONITOR'S REPORT NUMBER(S)

12. DISTRIBUTION/AVAILABILITY STATEMENT
Approved for public release: distribution unlimited.

13. SUPPLEMENTARY NOTES
ORCID IDs: Ngon T Tran, 0000-0002-5988-1784; Daniel B Knorr Jr, 0000-0003-3165-371X; Jennifer Sietins 0000-0003-2547-1653

14. ABSTRACT
Porosity quantification is a critical measurement for accurately determining material density and processing–microstructure–performance relationships. X-ray-computed tomography (XCT) and mercury infiltration porosimetry are complementary techniques that can be used to obtain a big picture of the internal void structure and progression at varied processing stages. However, each technique has its limitations, which will be discussed in detail within this report. Both glassy carbon foams and a 3-D carbon weave were used to study the instrument capabilities and measurement ranges. Percent porosity, bulk densities, and skeletal densities were directly compared, and explanations provided for discrepancies between them. Additionally, void sizes and location dependencies were quantified for XCT. This information can be used to discern which techniques would be better suited for specific samples of interest based on the expected void size range and, more importantly, to understand the accuracy limitations of the different methods.

15. SUBJECT TERMS
Sciences of Extreme Materials, carbon, mercury infiltration porosimetry, X-ray-computed tomography, porosity characterization

16. SECURITY CLASSIFICATION OF:			17. LIMITATION OF ABSTRACT	18. NUMBER OF PAGES	19a. NAME OF RESPONSIBLE PERSON
a. REPORT	b. ABSTRACT	c. THIS PAGE			Jennifer M Sietins
Unclassified	Unclassified	Unclassified	UU	25	19b. TELEPHONE NUMBER (Include area code) (410) 306-1949

Standard Form 298 (Rev. 8/98)
Prescribed by ANSI Std. Z39.18

Contents

List of Figures

List of Tables

1. Introduction

Carbon/carbon (C/C) composites are well known for their high performing mechanical properties, especially at elevated temperatures. These properties make the material an excellent candidate for applications such as heat shields or rocket nozzles that must maintain structural integrity while experiencing extreme temperatures. Increased porosity is one microstructural feature that can negatively impact mechanical performance. In particular, it has been reported that increased porosity reduces the transverse tensile strength of C/C composites.[1] Computational models for 2-D C/C have shown a significant increase in delamination and reduction in bending strength with increased porosity.[2] Also, the apparent shear strength in unidirectional C/C was reported to be drastically reduced with increased matrix porosity.[3]

There are numerous methods for quantifying porosity within a microstructure and each has advantages and disadvantages. Some common methods include the following: X-ray-computed tomography (XCT), mercury infiltration porosimetry (MIP), helium pycnometry, or serial section with optical microscopy. Each technique has different limitations for sample sizes and achievable resolution for pore size detectability. This study focuses strictly on XCT and MIP techniques for porosity quantification of carbon foams and a 3-D orthogonal C/C weave.

XCT is advantageous because it is a nondestructive technique that can be used to obtain information on both open- and closed-porosity in all three dimensions. Pore sizes, percent porosity, bulk and skeletal density can all be calculated from XCT data as well as location dependencies such as porosity through the thickness of the sample. Disadvantages of XCT include large up-front equipment costs, long scan or analysis times, and resolution limitations—which are generally linearly proportional to the scan field of view based on a fixed number of pixels across the detector.

MIP can readily detect much smaller pore sizes and has more automated quantitative results. A major drawback is that hazardous waste is generated; therefore, the ability to properly handle and dispose of mercury waste is very important. The analysis is much more automated than XCT and multiple samples can be run at once, depending on the number of sample chambers in the instrument. Depending on the geometry of the sample and the porosity within it, other considerations—such as closed porosity and small tunnels or channels between connecting pores leading to the “ink-bottle” effect—are necessary. This effect occurs when larger internal pores are only accessible through narrow channels, and the MIP misrepresents the pore size as equal to the size of the internal connections.[4]

This will be further explored and discussed in relation to the XCT results within this report.

Previous work by Weber et al., directly compared XCT and MIP for C/C composites; the pore size distribution was similar when considering pore sizes above their XCT scan resolution of 10 μm.[5] Expanding beyond Weber's work, this report summarizes additional analysis that can be conducted from XCT data sets to discern location and directional dependencies. A thorough discussion on the limitations of each technique and potential sources of error are also examined.

2. Procedure

2.1 Materials

Glassy carbon foams ranging from 10 pores per inch (ppi) to 100 ppi were purchased from Duocel to explore a wide range of pore sizes, determine instrument limitations, and readily compare the results. The foams were densified with six rounds of chemical vapor infiltration (CVI) in commercial-scale CVI furnaces employing a hydrocarbon feedstock. Cylindrical cores 12.7-mm in diameter were machined using a Drilax diamond-hole saw to provide appropriately sized samples for the subsequent porosity characterization methods. The XCT was conducted first and followed by the MIP on the same samples to limit sample-to-sample variability. Following the glassy carbon foam characterization, an as-received 3-D orthogonal weave manufactured by T.E.A.M., Inc. with AS4 carbon fiber tows was characterized using the same methods. This included a smaller sample 12.7-mm in diameter and a larger 31.75- × 31.75- × 12.7-mm rectangular sample.

2.2 XCT

A Zeiss Xradia 520 micro-computed tomography (μCT) system and NorthStar X5500 industrial system were used to scan all samples. The scan resolution is linearly proportional to the scan field of view due to a fixed number of pixels across the detector. Therefore, system and scan settings were used to quantify both the porosity between tows and within the tows to assess scan-resolution limitations on the porosity quantification. Approximate sample sizes and scan settings are summarized in Table 1.

Table 1 Scan settings for foams and C/C weave samples analyzed

Sample description	Approximate dimensions	Scanner	keV	Number of projections	Voxel size (µm)
Foams	12.7-mm diameter	Zeiss Xradia 520	50	1601	16.37
C/C cylinder core (lower resolution)	12.7-mm diameter	Zeiss Xradia 520	60	2401	15.74
C/C cylinder core (higher resolution)	12.7-mm diameter	Zeiss Xradia 520	60	3201	3.39
C/C weave	31.75-mm wide	NorthStar X5500	85	1800	46.8

The foam-analysis module in Volume Graphics (VG) was used to quantify pore volumes and surface areas. This module is intended for open-celled foams, so it worked very well for analysis of the glassy carbon foams; however, other analysis methods were needed for the carbon weave. Therefore, Computed Tomography-Analyzer (CTAn) software* was used to quantify the following components of the microstructure that were of interest for both the foams and the 3-D weave: percent porosity, bulk and skeletal volume, and void volumes (only applicable to the 3-D weave).

2.3 MIP

Micrometrics AutoPore V 9600 was used to determine percent porosity and porosity size of open pores on the cylindrical XCT samples as well as to calculate bulk and skeletal densities. The penetrometer was evacuated to a pressure of 0.0003 MPa (0.05 psia) prior to filling with mercury to 216.7229 MPa (31,433 psia) over 494 logarithmically spaced intrusion pressures (i.e., from 0.01 psia at the beginning to 600–1200 psia at the end). For each pressure, the sample was allowed to equilibrate for 30 s and the maximum intrusion was 0.010 mL/g. The pressure at which the penetrometer is transferred from a low-pressure chamber to a high-pressure chamber is 40 psia, and care was taken to minimize any pressure generated during tightening of the high-pressure chamber. Immediately after the low-pressure analysis, the input for current "atmospheric pressure" was measured by the low-pressure transducer when the low-pressure port was opened. The advanced and receding contact angles were 155 °C.[6]

* Bruker MicroPhotonics

3. Results

3.1 Glassy Carbon Foams

Three-dimensional volume renderings of the glassy carbon foam µCT scans were imaged with CTVox software and are shown in Fig. 1. The qualitative differences between the pore sizes and overall porosity percentages are evident. These were selected to have distinct differences in bulk and skeletal densities as well as to establish instrument limitations based on the sizes of the microstructural features.

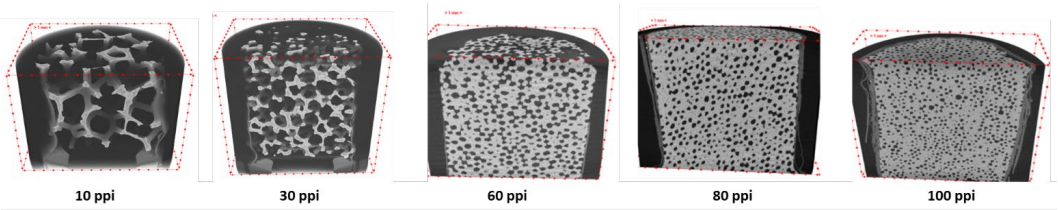

Fig. 1 The 3-D volume renderings of 10–100 ppi from left to right (spacing between red dots is 1 mm and all samples are 12.7-mm diameter)

3.1.1 Foam Percent Porosity

Quantification of the porosity for both the µCT and MIP methods are shown in Table 2. There is relatively close agreement in the percent porosity values for the higher density foams of 100, 80, and 60 ppi. The percent porosity for the foams follows the expected trend of increasing percent porosity with a lower number of pores per inch for the µCT analysis. The MIP results were not able to measure an accurate percent porosity in the lower density foams due to the very large openings of the pores with a very low number of pores per inch. This is likely due to the ease of infiltration of the mercury into the large openings, which led to an inaccurate bulk volume quantification, especially for samples containing pores that were opened at two or more locations on the surface.

Table 2 Glassy carbon foam percent porosities quantified for both µCT and MIP

ppi	Average porosity (%)	
	µCT	MIP
100	17.23	17.21
80	17.68	19.50
60	32.86	26.97
30	70.06	(0.96)
10	86.78	(1.94)

3.1.2 Foam Skeletal and Envelope Densities

Skeletal densities were calculated by dividing the mass over the volume of the solid material (including closed pores but excluding open pores). As expected, the skeletal densities had little variability between the foams because the density of the carbon phase remained the same among the samples. Results are shown in Fig. 2. Calculated skeletal densities were similar between the µCT and MIP, with the µCT consistently measuring slightly higher densities than the MIP method. This might be caused by a slight underestimation of the µCT volumes due to cropping near the base of the sample where the foams were touching the top of the mount fixture.

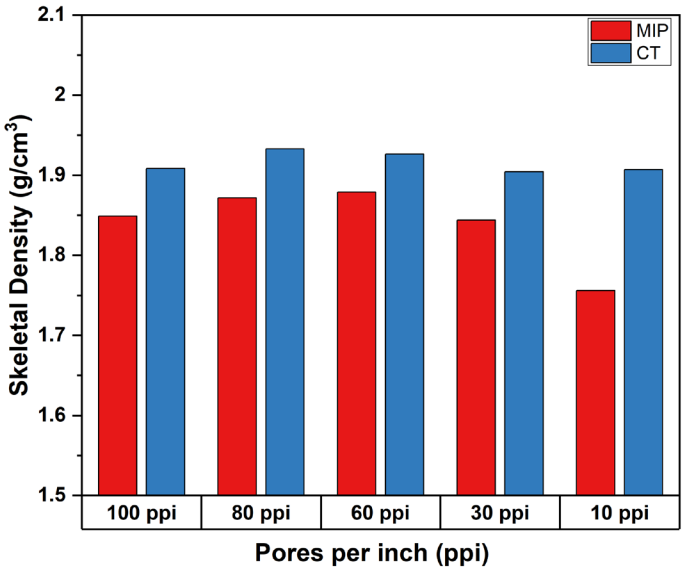

Fig. 2 Skeletal densities of open-celled carbon foams measured with µCT and MIP

Similarly, envelope densities were quantified by dividing the mass over the total cylindrical volume, which included all pores. Figure 3 shows the results were similar for higher density foams (100 and 80 ppi). It was evident that the pore sizes were too large for the MIP to measure the envelope density at the lower foam densities of 10 and 30 ppi because the pore sizes were larger than the maximum range of the MIP instrument.

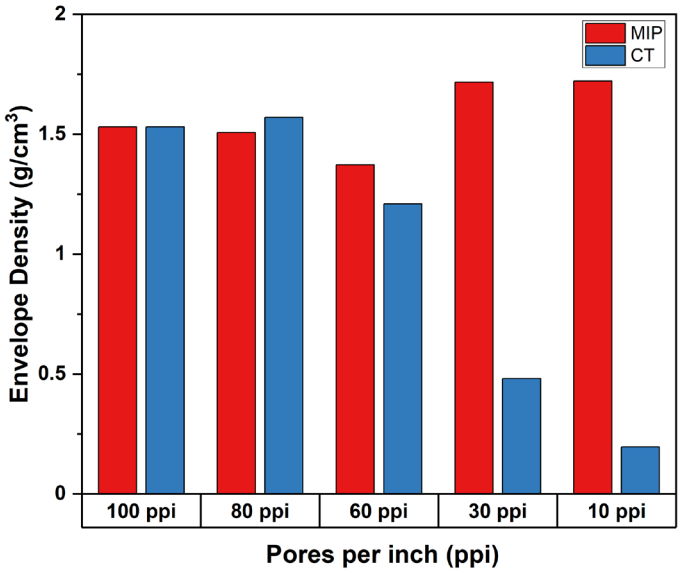

Fig. 3 Envelope densities are in close agreement for the higher density foams (100 and 80 ppi in particular), whereas very low density foams (30 and 100 ppi) have pore sizes that are too large for the MIP to measure

3.1.3 Foam Pore Diameters

Pore diameters were quantified for the XCT data, MIP results, and theoretical values, as shown in Fig. 4. VG software and the foam-analysis module were used to quantify pore diameters for the open-celled foams for the XCT results, both including and excluding pores that are on the outer edge of the cylinder. Pores on the outer edge are cut into a smaller fraction; therefore, including them skews the average pore diameter to a smaller value, particularly for foams with larger pore sizes. Theoretical values were calculated by simply dividing 25.4 mm by the number of pores per inch. This is a very simplistic estimate as it is not considering the ligament thicknesses. The pore diameter from the MIP data was taken as the histogram peak of the cumulative intrusion (mL/g) versus diameter plot.

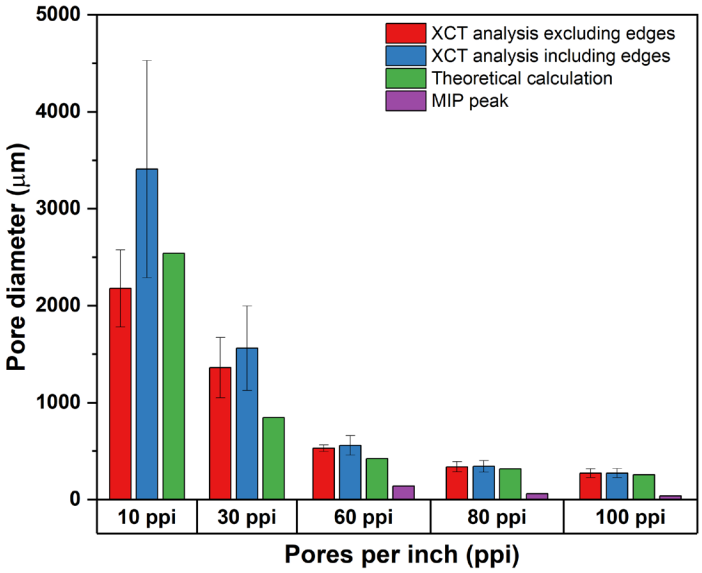

Fig. 4 Pore diameters quantified from µCT, MIP, and theoretical calculations

The 10-ppi results for the XCT data were above and below the theoretical value when excluding and including the pores on the outer edges, respectively. The 30-ppi results did not closely match the theoretical calculation, which is likely due to the theoretical calculation not accounting for the ligament thickness, solid fraction of the foam, or the smaller number of pores analyzed for the same sample volume. The 60–100 ppi foams all had over 2,000 pores analyzed, whereas the 10 and 30 ppi foams had less than 500 total pores. The 60-, 80-, and 100-ppi results matched fairly close for the XCT and theoretical values; the edge effects had significantly less impact due to the smaller pore sizes and large number of pores per unit volume. For the MIP peak results, the 10 and 30 ppi were not expected to match with either the theoretical values or XCT data based on the void sizes being larger than the upper limit for the MIP instrument, which is 500 µm—as evidenced in the earlier percent porosity errors. The higher density foam MIP results were not close to either the theoretical values or the XCT results, which we suspected was due to the "ink-bottle" effect and the smaller pore window openings between pores (as demonstrated in Fig. 5, left). At a lower pressure, the mercury infiltrates the small pore and stops at the red-dashed line until reaching a high enough pressure to infiltrate the much smaller channel connecting the small and large pores. The higher pressure measured by the instrument prior to infiltrating the large pores leads to a significant underestimation of the pore sizes. See the right image in Fig. 5 of the 60-ppi sample. The pore window openings range between 35 and 169 µm, which are significantly smaller than the pore sizes.

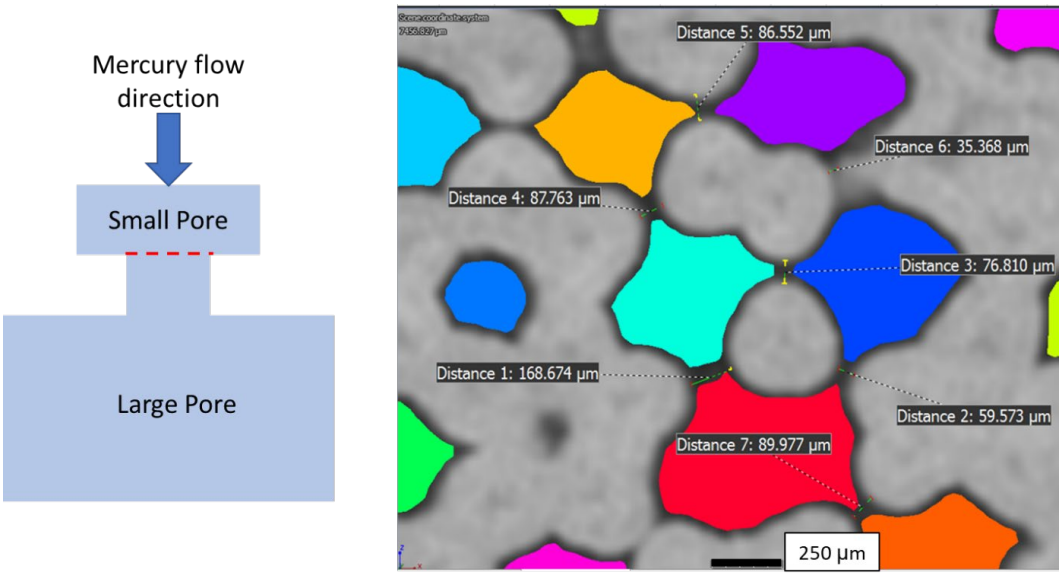

Fig. 5 The "ink-bottle" effect (left) and measurements of pore window sizes between pores on the 60-ppi sample (right)

To test this theory, 3-D pore window analysis was conducted in the VG foam-analysis module to automatically quantify the opening sizes between neighboring pores. As shown in Fig. 6, the average face diameter is much closer to the MIP peak, especially for the 80 and 100 ppi foams that have more pores per volume and a lower standard deviation. The pore window quantification being on the order of the MIP peak is a strong indication that the "ink-bottle" effect is the reason for the underestimation of the pore diameter sizes with the MIP instrument.

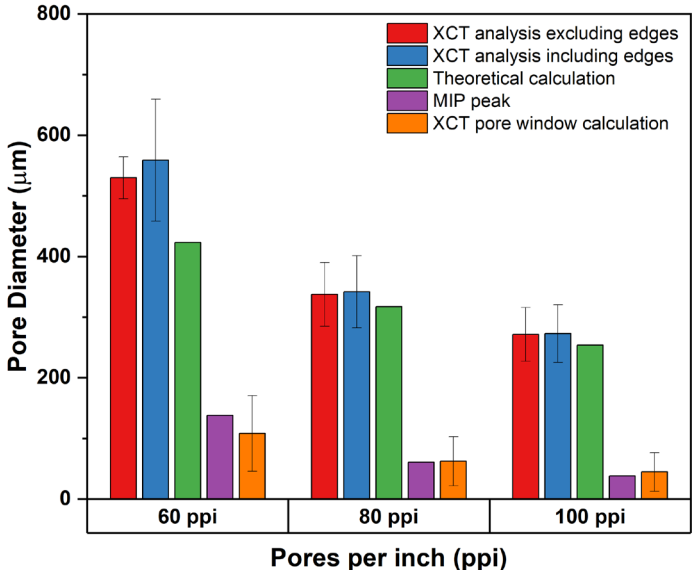

Fig. 6 Pore size diameter results, including the measurement of pore window sizes between connecting pores

In summary, for the glassy carbon foams, the XCT and MIP measured very similar skeletal densities for the entire range of pore sizes. The envelope densities, however, were only comparable for the higher density foams of 60–100 ppi. This was due to the pore sizes being larger than the upper limit of the MIP measurement range and the mercury readily flowing into the large pores and inaccurately measuring the sample volume. The pore diameters measured with the XCT and VG software were relatively close to the theoretical values based on the total number of pores per inch. The MIP, however, significantly underestimated the pore diameters for all pore sizes. This was hypothesized to be caused by the "ink-bottle" effect and the smaller sizes of openings between the neighboring pores. This was confirmed through analyzing the face diameters, which were much closer to the MIP pore diameter results.

3.2 Woven C/C Preform

3.2.1 C/C Percent Porosity

The C/C preform percent porosity was measured in a similar fashion as the open-celled foams. CTAn was used to quantify the percent porosity, which is shown with the MIP results in Table 3. The XCT percent porosity was significantly lower than the MIP, which we hypothesized to be caused by the high frequency of small pores below the resolution limit of the XCT instrument. Typical feature detectability is about 3–5× the pixel (2-D) or voxel (3-D) of the scan.[7] Therefore, with a scan voxel size of 15.74 μm, void-size detectability would be on the order of 50 μm or larger. This is sufficient for detecting the large voids between tows, but not for readily detecting the small voids within the tows.

Table 3 Percent porosity calculated from μCT scan and MIP on a C/C orthogonal weave

Sample	Average porosity	
	XCT	MIP
C/C weave	20.96	45.98

To check this hypothesis, truncation of the raw MIP data was employed to calculate the percent porosity for mercury intrusion above the 50-μm threshold. A similar procedure was used by Weber et al.,[5] which demonstrated close agreement between the XCT and MIP when restricting the MIP pore sizes to the resolution limit of the XCT scans or larger. Equation 1 was used to quantify the truncated percent porosity from the raw MIP data:

$$Truncated\ \%\ Porosity = \left(1 - \frac{\text{Cumulative Intrusion}_{Max} - \text{Cumulative Intrusion}_{50\ um}}{\text{Cumulative Intrusion}_{Max}}\right) * Total\ \%\ porosity \qquad (1)$$

This resulted in a percent porosity of 18.74%, which is much closer to the XCT calculated percent porosity.

3.2.2 C/C Skeletal and Envelope Densities

Table 4 summarizes the results for the skeletal and envelope densities of the orthogonal C/C weave. The envelope densities were all similar. A possible explanation for the deviation in the skeletal densities is the resolution limit of the XCT scans. A lower resolution would result in a larger skeletal volume and therefore a lower skeletal density. Also, the high frequency of very small voids (within the tows and <50 μm in size) likely contributes to an underestimation of the skeletal density. The percent porosity shown in Table 3 is evidence that there is a very high percent porosity that is below the XCT scan resolution. Further, the μCT results of 15.74 μm had a higher skeletal density compared to the industrial XCT results with a voxel size of 46.8 μm. Therefore, skeletal densities measured with XCT may be underestimating the skeletal density and MIP would be the recommended method if this value was important to accurately measure.

Table 4 Skeletal and envelope densities measured with XCT (15.74- and 46.8-μm voxel sizes) and MIP

Measurement technique	Skeletal density	Envelope density
μCT (15.74 μm)	1.257	0.927
CT (46.8 μm)	1.175	0.918
MIP	1.8235	0.9851

3.2.3 Advanced CT Analysis

Additional analysis can be conducted on the XCT data sets to obtain information regarding the size and location deviations within the sample. This information is valuable for quantifying porosity reduction at variable processing stages, especially for determining the potential effectiveness of subsequent CVI cycles. The “2-D Analysis” feature in the CTAn software quantifies the porosity as a function of through-thickness depth. Figure 7 (left) shows differing porosity percentages around 15% and 25%, which corresponds to the warp and weft directions, respectively. This is visually illustrated in the images shown in Fig. 7 (right).

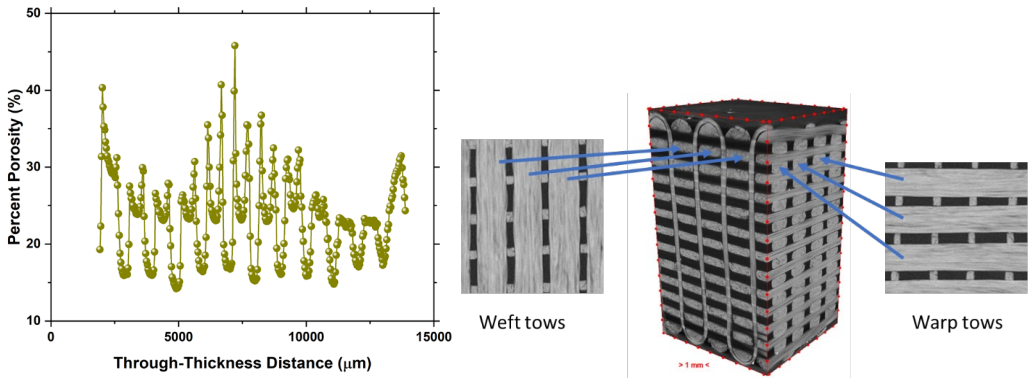

Fig. 7 Porosity as a function of through-thickness distance shows variability between warp and weft tows (left), and 3-D volume rendering with 2-D cross-sectional images demonstrate size differences in the voids between weft and warp tow directions (right)

3.2.4 XCT Quantification of Void Sizes

Advanced segmentation of voids between tows can be accomplished with image-processing functions such as erosion and dilation to separate touching pores, which are predominantly located at the intersection of the 0°/90° fiber tows. A 3-D model of a successful segmentation is shown in Fig. 8 (left). The CTAn analysis called "individual object analysis" was conducted to quantify the size and location of each of the segmented voids. The exported data included volumes, surface areas, position centroids, and equivalent spherical diameters for each of the voids. Figure 8 (right) plots the equivalent diameter as a function of through-thickness height. It is evident that the voids between warp tows are consistently larger than the voids between the weft direction. This is important information when exploring directional dependencies within composites, such as thermal or mechanical performance. Also, knowing the dimensional differences at different directions assists in the development of more accurate models for simulation purposes.

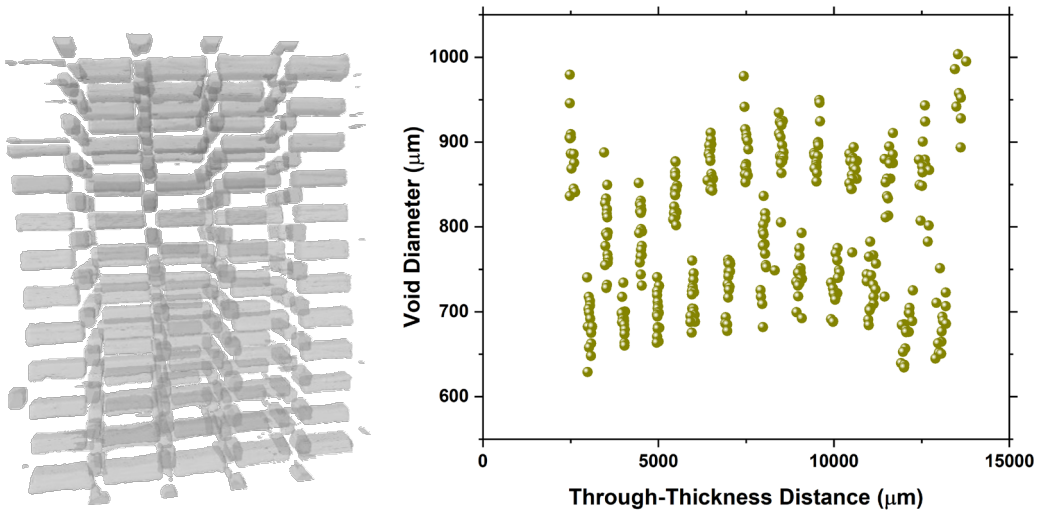

Fig. 8 A 3-D model illustration of successful segmentation (left) and void volumes as a function of the void centroid through the thickness of the panel (right)

Equivalent diameters were also calculated assuming a cylindrical shape and using the Gurwitch rule (4× the volume divided by the surface area) to be consistent with the MIP calculated diameters. Histograms of these equivalent diameters showed a bimodal distribution (Fig. 9). This was independently validated by manually measuring the dimensions of a single void parallel to the warp and weft tows and calculating the equivalent cylindrical diameters with the 4 V/S formula. Those diameters were quantified as 419 and 338 μm, respectively, which agrees nicely with the histogram results. The MIP did not capture the bimodal distribution and also underestimated the void diameter, which is likely due to the "ink-bottle" effect and the instrument increasing to a higher pressure to infiltrate between the small gaps between the 0°/90° tow intersections. This is similar to the foam window sizes underestimating the pore sizes (as discussed previously).

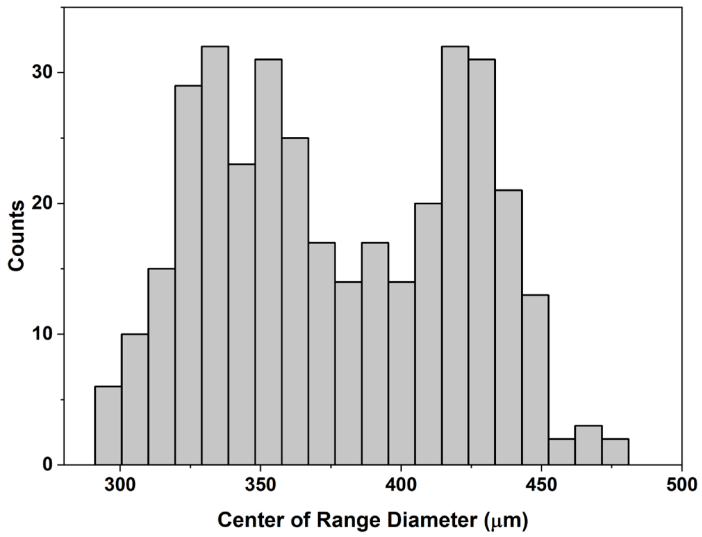

Fig. 9 Histogram of equivalent diameters showing bimodal peaks for voids between the warp and weft tow directions

Similar histograms were also generated for the high-resolution (3.39-μm) scan to quantify voids within the tows. Six different tows were analyzed (three warp and three weft). All showed a similar range of calculated void diameter sizes between 5 and 12 μm, as shown in a representative histogram in Fig. 10 (left). This is in good agreement with the MIP peak for the voids within the tows as shown in Fig. 10 (right). This agreement is attributable to the lack of "ink-bottle" effect for these voids within the MIP since the larger voids are infiltrated first at lower pressures. Mercury only flows through these small voids within the tows at higher pressures within them—thus, opening to larger, unfilled void pockets. For the XCT scan, the field of view was very small (~3.5 mm); therefore, both the analysis of voids between tows and voids within the tows are not possible to obtain statistically meaningful results within a single data set.

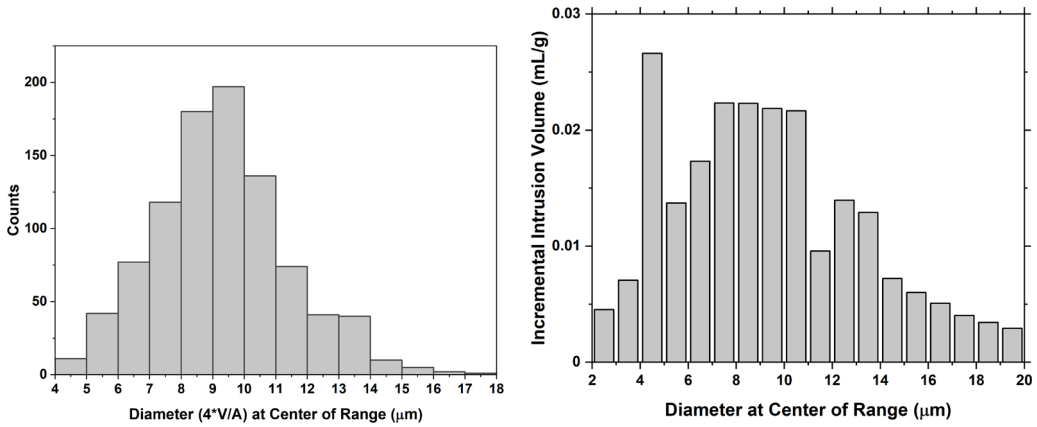

Fig. 10 Histogram of the voids within the tows from the high-resolution (3.39-μm) XCT scan (left), and MIP incremental intrusion vs. pore diameter (right) show good agreement for the void sizes within the tows

4. Discussion

As discussed throughout this report, there are numerous pros and cons to each methodology. Together, both techniques can be utilized to obtain more information about porosity over a larger range of sizes. One of the biggest differences between the two methodologies is that XCT is nondestructive and non-hazardous, whereas the mercury infiltration in the MIP process generates toxic waste and necessitates proper disposal. XCT can determine size, shape, type (open vs. closed), and location dependencies that MIP is not able to detect. XCT, however, is limited in the pore size detectability that is predominantly related to the scan field of view and sample size. Table 5 summarizes the primary considerations for the two techniques.

Table 5 Summary of major considerations for XCT and MIP porosity characterization

Attribute	μCT	MIP
Nondestructiveness	✓	×
Non-hazardous	✓	×
3-D pore structure and location	✓	×
Density mismatch requirement	✓	×
Detection of closed pores	✓	×
Pore diameter range[a]	>3× voxel size	500.0–0.005 μm
Measurement time[b]	>1 h	5 h
Post-measurement analysis	extensive	minimal

[a] Range depends on voxel size used for μCT and on the maximum pressure applied for MIP.
[b] Analysis time depends on voxel size used for μCT and on the parameters (e.g., equilibrium time, number of pressure points, and maximum intrusion for each pressure point) used for MIP

The pore diameter detectability and scan times vary significantly for XCT and depend on numerous factors. The voxel size is one of the most important factors for the scan resolution; however, other scan settings influence the sharpness of feature edges, the level of background noise in the image, and contrast between phases of different densities. Each of these factors influence both the scan time and the resulting quality of the image, which impacts the ability to successfully segment and quantify porosity. Scan times can easily range from approximately 1 h to 12+ h, predominantly based on the scan resolution and the exposure time needed per projection image. Also, the post-scan analysis takes significantly more time than the MIP; however, future machine-learning algorithms, computational advancements, and automated image-analysis programs may significantly reduce the manual analysis time.

5. Conclusions

XCT has shown to be an excellent technique for measuring voids between tows. Higher resolution scans can quantify voids within the tows; however, this is limited to a very small field of view and also long scan times. Another major advantage of the XCT technique is the ability to determine spatial dependencies (i.e., porosity through the thickness of the composite or variability in sizes between warp and weft directions). MIP is an excellent technique for measuring smaller voids within the tows that are well below the spatial resolution of the XCT. Both techniques are highly complementary to obtain a full picture of the pore size distribution of C/C composites, especially for voids between tows and within the tows.

In general, it is recommended to use MIP when:

- hazardous waste generation and disposal is not a concern;
- higher resolution porosity quantification (i.e., pores within tows) is desired;
- faster, automated analysis is important;
- directional dependencies are not of interest; and
- underestimation of large pores that are only connected via small channels (“ink-bottle” effect) is acceptable.

And it is recommended to use XCT when:

- information on large voids between fiber tows are of primary interest;
- directional information is desired, such as porosity through the thickness;
- longer scan or analysis times are acceptable;

- nondestructive evaluation is a priority; and
- 3-D images are needed to feed computational modeling.

Both techniques resulted in the same bulk-density quantification and percent porosity for the larger pores above the XCT resolution limit (when truncating the MIP data to match the XCT detectability limit). Therefore, both techniques can provide valuable information regarding densification of C/C composites after undergoing subsequent processing cycles, such as multiple chemical-vapor infiltration runs. This information can be used for optimizing resin chemistries or determining relationships between pore size/distribution with mechanical properties.

6. References

1. Brassell GW, Horak JA, Butler BL. Effects of porosity on strength of carbon-carbon composites. J Compos Mater. 1975;9(3):288296.

2. Chao X, Qi L, Tian W, Hou X, Ma W, Li H. Numerical evaluation of the influence of porosity on bending properties of 2D carbon/carbon composites, Compos B Eng. 2018;136:72–80.

3. Casal E, Granda M, Bermejo J, Bonhomme J, Menéndez R. Influence of porosity on the apparent interlaminar shear strength of pitch-based unidirectional C–C composites. Carbon. 2001;39(1)73–82.

4. Abell AB, Willis KL, Lange DA. Mercury intrusion porosimetry and image analysis of cement-based materials. J Colloid Interface Sci. 1999;211:39–44.

5. Weber E, Fernandez M, Wapner P, Hoffman W. Comparison of X-ray micro-tomography measurements of densities and porosity principally to values measured by mercury porosimetry for carbon–carbon composites. Carbon. 2010;48(8):2151–2158.

6. León y León CA. New perspectives in mercury porosimetry. Adv Colloid and Interface Sci. 1998;76–77:341–372.

7. Patterson BM, Dennis-Koller D, Cerreta E, Escobedo JP. Dimensional quantification of embedded voids or objects in three dimensions using X-ray tomography. Microsc Microanal. 2012;18(2):390–398.

List of Symbols, Abbreviations, and Acronyms

2-/3-D	two-/three-dimensional
ARL	Army Research Laboratory
C/C	carbon/carbon
CTAn	Computed Tomography-Analyzer
CVI	chemical vapor infiltration
DEVCOM	US Army Combat Capabilities Development Command
μCT	micro-computed tomography
MIP	mercury infiltration porosimetry
ppi	pores per inch
VG	Volume Graphics
XCT	X-ray-computed tomography

1 DEFENSE TECHNICAL
(PDF) INFORMATION CTR
DTIC OCA

1 DEVCOM ARL
(PDF) FCDD RLD DCI
TECH LIB

9 DEVCOM ARL
(PDF) FCDD RLW MA
JJ CAIN
DB KNORR JR
JM SANDS
NT TRAN
FCDD RLW MB
WH GREEN
KW KLAFF
BM LOVE
JM SIETINS
TW WALTER